Energetic neutral atom observations of magnetic anomalies on the lunar surface

A. Vorburger,[1] P. Wurz,[1] S. Barabash,[2] M. Wieser,[2] Y. Futaana,[2] M. Holmström,[2] A. Bhardwaj,[3] and K. Asamura[4]

[1]   SARA, the Sub-KeV Atom Analyzer, on board Chandrayaan-1 recorded the first image of a minimagnetosphere above a lunar magnetic anomaly using energetic neutral atoms (ENAs). It was shown that this magnetosphere, which is located near the Gerasimovich crater, is able to reduce the solar wind ion flux impinging onto the lunar surface by more than 50%. Following this first observation, we investigated all magnetic anomalies that are in the SARA data set. We searched for a possible correlation between the solar wind plasma parameters (dynamic pressure, magnetic field), the local magnetic field, and the reduction in the reflected hydrogen ENA flux (henceforth called shielding efficiency). Having analyzed all observations by SARA, we discovered that the Gerasimovich magnetic anomaly is topologically a very simple, large-scale magnetic structure, which is favorable for this kind of investigation. Most other magnetic anomalies on the lunar surface have more small-scale features in their magnetic field structure, which complicates the interpretation of the observed data. We find a clear correlation between the plasma parameters and the shielding efficiency for the Gerasimovich case. For the other observed anomalies only about half of the cases showed such a correlation. We therefore conclude that the solar wind ions-magnetic anomaly interaction is in general more complex than in the Gerasimovich case.

1. Introduction

[2]   The Moon does not posses a global magnetic field as for example Earth, Mercury and Jupiter do. After the first lunar landing with Apollo 11, though, *Runcorn et al.* [1970] discovered that samples returned from the Moon showed remanent magnetization. In the same year, *Dyal et al.* [1970] reported on measurements by the Apollo 12 magnetometer, which showed that a permanent localized magnetic field exists at the Apollo 12 landing site. Having analyzed the measurements of remanent magnetic fields at four Apollo landing sites, *Dyal et al.* [1972] found that there was a strong correlation between the magnetic field strength and the solar wind plasma density and that the remanent magnetic field was compressed as much as 40% above its initial value by the solar wind. *Russell and Lichtenstein* [1975] investigated the source of lunar limb compressions using Apollo 15 and 16 sub-satellites data. They state that the most probable cause of limb compression is the deflection of the solar wind by the lunar surface magnetic field. Almost 30 years later, *Lin et al.* [1998] studied more thoroughly the interaction between the solar wind electrons and regions of strong crustal magnetic fields using Lunar Prospector magnetometer and electron reflectometer data. They concluded that the crustal magnetic fields of the Imbrium antipode region may be strong enough to deflect the solar wind to form a minimagnetosphere. In addition, they found implications that at least some of the surface magnetic fields should be able to stand off the solar wind. 2.5D MHD simulations by *Harnett and Winglee* [2002] support the theory that minimagnetospheres are formed and that they can hold off the solar wind. *Kurata et al.* [2005] analyzed the Reiner Gamma anomaly region under different solar wind conditions using Lunar Prospector magnetometer data. They showed that the size and the shape of the minimagnetosphere are expected to strongly depend on the solar wind conditions. *Futaana et al.* [2006] predicted that a signature of a magnetic anomaly should be detectable in ENA observations of atoms sputtered from the lunar surface: Since the solar wind ions are deflected above the magnetic anomaly and fewer ions enter the anomalous region, less ENAs should be sputtered from that area than from its unmagnetized neighborhood. *Wieser*

---

[1]Physikalisches Institut, University of Bern, Bern, Switzerland.
[2]Swedish Institute of Space Physics, Kiruna, Sweden.
[3]Space Physics Laboratory, Vikram Sarabhai Space Center, Trivandrum, India.
[4]Institute of Space and Astronautical Science, Sagamihara, Japan.

Corresponding author: A. Vorburger, Physikalisches Institut, University of Bern, Sidlerstrasse 5, CH-3012 Bern, Switzerland. (vorburger@space.unibe.ch)

et al. [2010] confirmed this hypothesis by producing the first image of a lunar magnetic anomaly in backscattered hydrogen atoms measured by the Chandrayaan-1 Energetic Neutral Analyzer (CENA). The hydrogen atoms were coming from an area close to the Gerasimovich crater (= Crisium antipode) where a strong magnetic anomaly is located. Mapping of Lunar Prospector magnetometer and Electron Reflectometer data [see, e.g., *Mitchell et al.*, 2008; *Richmond and Hood*, 2008] showed that the Moon is strewn with regions exhibiting high magnetic field strengths.

[3] We analyzed all CENA observations of magnetic anomalies on the lunar surface to see if 1) a signature of the magnetic anomaly is always visible in the ENA signal and if 2) there is a correlation between the solar wind dynamic pressure, the solar wind magnetic field, the local magnetic field strength and the reduction in the reflected ENA flux. Since the magnetic anomaly at the Gerasimovich crater proves to be such a good study case, we first analyze all observations of the Gerasimovich crater, before we expanded our analysis to cover the other observed magnetic anomalies.

2. Instrumentation and Data Set

[4] Chandrayaan-1 was the first Indian mission to the Moon [*Goswami and Annadurai*, 2009]. The mission lasted from October 2008 until the end of August 2009. The spacecraft was initially inserted into a 100 km circular polar orbit, which was raised to 200 km at the end of May 2009. The spacecraft carried, amongst ten other scientific instruments, the SARA instrument [*Bhardwaj et al.*, 2005; *Barabash et al.*, 2009], on the results of which we will report here. SARA was in operation from the end of January until the end of July 2009. SARA consists of two sensors, CENA, the Chandrayaan-1 Energetic Neutral Analyzer, and SWIM, the Solar Wind Monitor, and a digital processing unit (DPU). SWIM measures ions in the energy range of 10 eV–15 keV, which are of solar wind and lunar origin, whereas CENA measures lunar ENA. CENA's energy range covered particles within the range 10 eV–3.3 keV with an energy resolution of 50%. CENA consists of seven angular sectors each with a field-of-view of $45° \times 6.44°$ ($FWHM_{azimuth} \times FWHM_{elevation}$). The central sector (sector number 3, henceforth) is pointing in the nadir direction. The other 6 sectors are arranged symmetrically around sector 3 with azimuthal angular separations of $\pm19°$ (sectors 2 and 4, respectively), $\pm38°$ (sectors 1 and 5, respectively) and $\pm57°$ (sectors 0 and 6, respectively). *Wieser et al.*'s [2010, Figure 1] illustrates the arrangement of the five central sectors. Note that sectors 0 and 6 both see the lunar surface as well as the lunar limb. They are therefore not illustrated in *Wieser et al.* [2010, Figure 1] and were not used in this analysis. The surface projections of the central five field-of-views correspond to 83×11 km^2 (sector 3), 97×11 km^2 (sectors 2 and 4) and 169×11 km^2 (sectors 1 and 5) for a 100 km orbit and to 168×23 km^2 (sector 3), 198×23 km^2 (sectors 2 and 4) and 416×23 km^2 (sectors 1 and 5) for a 200 km orbit. We only analyzed the hydrogen ENAs in the energy range 150 eV–600 eV, since *Wieser et al.* [2010] showed that the magnetic anomaly signature is strongest for these species. The integration time for one measurement equals ~4 s and the time required for one orbit was about 2 hr. For our analysis we only used data obtained within

$\pm60°$ of the equator during day-side observations. The reason for the exclusion of higher latitudes is that the flux decreases rapidly with increasing latitude until it comes close to CENA's detection limit. To take the varying magnitude of the solar wind ion flux (which directly influences the magnitude of the measured ENA flux) into account, we divided the measured ENA flux by the solar wind proton flux. Due to spacecraft power considerations, SWIM and CENA were not always running concurrently. To not have to exclude any data sets due to this limitation we chose not to use SWIM data but data from the WIND spacecraft to determine the solar wind parameters. Since WIND is located at the Lagrange-1 point we had to time-shift the WIND measurements according to the distance between WIND and Chandrayaan-1 and according to the solar wind ions' velocity.

[5] We analyzed the day-side data of 87 orbits, which gives us 435 data sets (87 orbits × 5 sectors). During these orbits, the five central sectors conducted 121 observations of 10 different magnetic anomaly regions. These are all observations of lunar magnetic anomalies that are contained in the CENA data set. Figure 1 depicts the magnetic anomaly regions which were observed. We used the global map of the total magnetic field strength at an altitude of 30 km presented by *Richmond and Hood* [2008, Figure 7] for context. Encircled and labeled are the regions on which we will report.

3. Data Analysis

[6] To determine an anomaly's shielding efficiency (the percentage by which a magnetic anomaly is able to reduce the backscattered ENA flux), we first had to fit our normalized ENA flux with the angular scattering function of solar wind protons backscattered as ENAs presented in *Schaufelberger et al.* [2011] to obtain a reference curve for comparison. The scattering function comprises of four ad hoc functions, each of which describes the variation of one of the following observed features: (1) amplitude, (2) azimuthal uniformity, (3) ratio of sunward versus antisunward flux, and (4) mean polar scattering. Whereas the first feature is solely a function of solar zenith angle, features (2) and (3) are functions of the solar zenith angle and the azimuthal scattering angle and feature (4) is a function of solar zenith angle and elevation scattering angle. Since the scattering function is only a function of the solar zenith angle and the polar and azimuthal scattering angles it is well defined for each orbit and each observation geometry along the orbit. The ENA scattering function describes the angular scatter of impacting solar wind ions for a lunar surface that is smooth and globally homogeneous. This is of course only a very crude approximation for the lunar surface. The actual lunar surface will show local variations in the backscatter efficiency due to local variations in the surface structure and mineralogical composition.

[7] The normalized ENA flux and the scattering function are linked to each other by the sub-solar reflection ratio [*Schaufelberger et al.*, 2011], for which the global average value has been recently evaluated to be $0.19^{+0.02}_{-0.03}$ [*Futaana et al.*, 2012]. Since we are interested in the local variation of the ENA flux we fitted the amplitude of the scattering function to the data, which is the only fit parameter in this
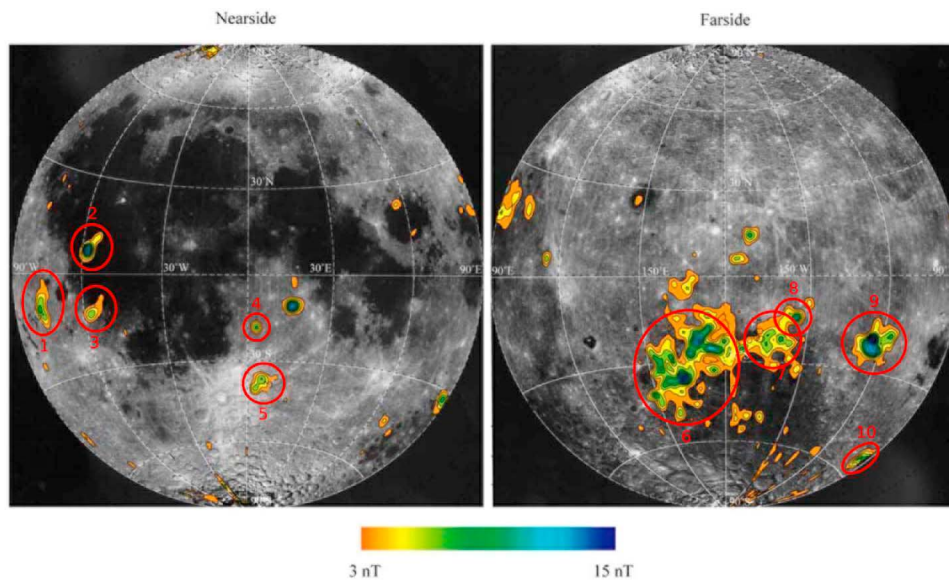
Figure 1. The different magnetic anomaly regions observed by CENA are encircled and labeled. The colored and the albedo background images are taken from *Richmond and Hood* [2008]. The colored background image presents a global map of the total magnetic field strength at an altitude of 30 km measured by the Lunar Prospector magnetometer and the background albedo image is the Clementine albedo map.

procedure. Because of local variations in ENA backscatter efficiency, we sometimes had to de-trend data from some orbits. The de-trending is accomplished by minimizing the difference between the normalized ENA flux and the scattering function through a polynomial of 3rd degree, which only removes large scale fluctuations.

[8] We then compared our ENA flux to the total magnetic field strength measured by the Lunar Prospector magnetometer at an altitude of 30 km and presented by *Richmond and Hood* [2008]. Figure 2a shows the integral neutral hydrogen flux from a surface element derived from the CENA measurements on 17 June 2009 using the angular scattering function [*Schaufelberger et al.*, 2011] and applying a normalization with the solar wind proton flux. Figure 2b shows a gray scale albedo map provided by the Clementine spacecraft for context, and Figure 2c the magnetic field strength measured by the Lunar Prospector magnetometer at an altitude of 30 km [*Richmond and Hood*, 2008].

[9] The initial observations by *Wieser et al.* [2010] show that there is a significant reduction of the ENA flux above a magnetic anomaly, and that there is a region of enhanced ENA flux surrounding the depression. The latter presumably arising from the deflection and concentration of the solar wind ions by the magnetic field. We therefore divided the ENA signal up into 3 regions: 1) undisturbed region 'U' (where the crustal magnetic field $B_{\mathrm{Moon}} < 4$ nT), 2) inside minimagnetosphere 'M' ($B_{\mathrm{Moon}} > 4$ nT) and 3) enhanced ENA flux region 'E' (within $\pm 10°$ lunar latitude of region 'M', as observed at the Gerasimovich crater by *Wieser et al.* [2010]). We normalized the fitted scattering function to 1 and computed the shielding efficiency as:

$$SE(J_{\mathrm{ENA}}, J_{\mathrm{S}}) = 1 - \frac{J_{\mathrm{ENA}}}{J_{\mathrm{S}}}, \qquad (1)$$

where J_{ENA} is the ENA flux and J_{S} is the corresponding amplitude fitted scattering function. To determine the maximum value of the shielding efficiency, which we will present in the next section for each available orbit, we only looked at region 'M'.

[10] Figure 3 shows an example of the shielding efficiency for orbit 2659 (17 June 2009 20:53:27–23:01:00) versus lunar latitude. Figure 3a shows the value of the lunar magnetic field at an altitude of 30 km measured by the Lunar Prospector magnetometer [*Richmond and Hood*, 2008]. From this panel we determined the three regions 'U', 'M' and 'E', which are indicated in this and all following panels. Figure 3b shows the ENA flux normalized to the solar wind (solid) and the fitted scattering function (dashed), and Figure 3c shows the corresponding shielding efficiency $SE(J_{\mathrm{ENA}}, J_{\mathrm{S}})$.

[11] In a second step, we wanted to determine the uncertainty of a positive identification of the correlation of an ENA depression with a magnetic field peak. The uncertainty would be indicated by the variance of the shielding efficiency curve in the undisturbed region 'U'. But, as is obvious from Figure 3b, toward the lunar poles, as the ENA signal comes close to the detection limit, the ratio between the measured flux and the fitted scattering function is not well defined anymore, and the such derived uncertainty would be strongly overestimated. We therefore multiplied the shielding efficiency with the normalized fitted scattering function to obtain the normalized shielding efficiency:

$$SE_{\mathrm{norm}}(J_{\mathrm{ENA}}, J_{\mathrm{S}}) = \left(1 - \frac{J_{\mathrm{ENA}}}{J_{\mathrm{S}}}\right) \cdot \left(\frac{J_{\mathrm{S}}}{\max(J_{\mathrm{S}})}\right), \qquad (2)$$

where again, J_{ENA} is the ENA flux and J_{S} is the amplitude fitted scattering function. The normalized shielding efficiency is shown in Figure 3d). We finally defined the
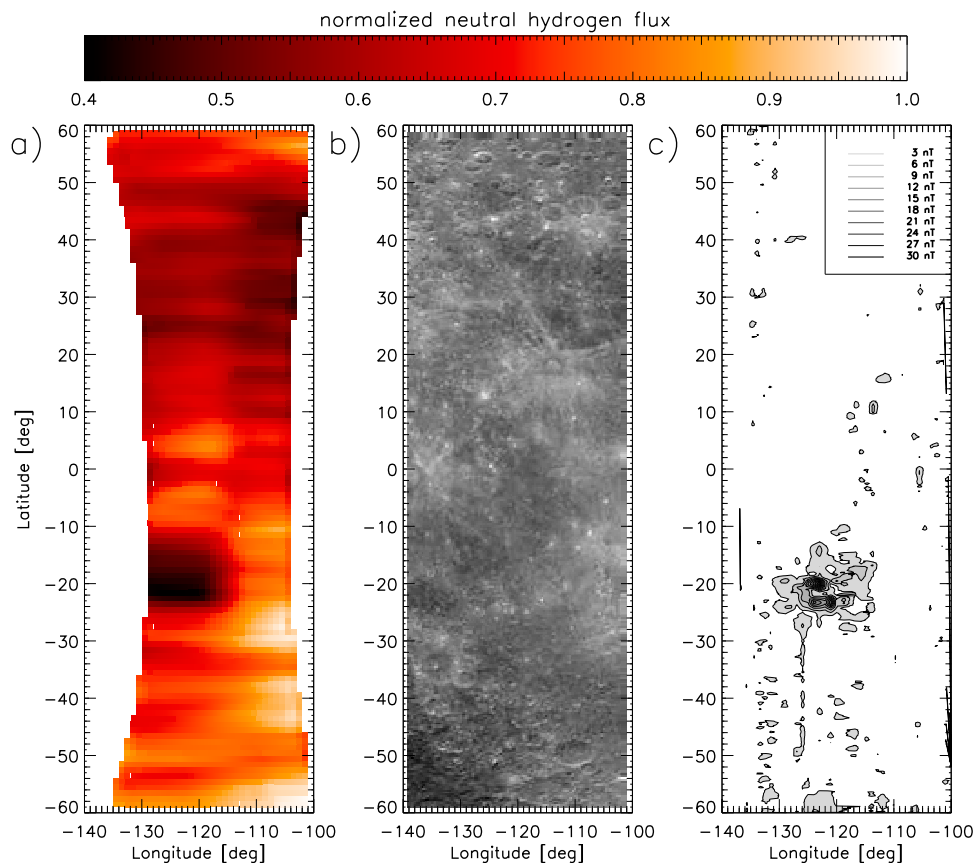
Figure 2. Observation of the magnetic anomaly near the Gerasimovich crater from 200 km altitude on 17 June 2009, with an albedo and a magnetic field strength map for context. (a) The measured integral neutral hydrogen flux using the angular scattering function and applying a normalization with the solar wind proton flux. (b) Gray scale albedo map provided by the Clementine spacecraft. (c) The magnetic field strength measured by the Lunar Prospector magnetometer at an altitude of 30 km.

uncertainty of the shielding efficiency as the variance of the normalized shielding efficiency in the undisturbed region 'U'. Thus, this uncertainty gives the likelihood that a fluctuation of the observed ENA flux, which is unrelated to the magnetic anomaly, is mistaken as a signature of the minimagnetosphere.

4. Results

[12] Near the Gerasimovich crater (location number 9 in Figure 1) we find the magnetic anomaly region on which *Wieser et al.* [2010] already reported. For the Gerasimovich anomaly we have by far the largest number of observations and the magnetic structure of the anomaly is relatively simple and of sufficient large geometric extent, so we chose to analyze this anomaly first. The Gerasimovich region was observed 37 times by the central five sectors of CENA. Out of these 37 observations, 32 showed a clear void in the 150 eV–600 eV hydrogen ENA signal when the magnetic anomaly was in the sector's field-of-view. We divided these 32 cases up into two groups: Group 1 contains the observations where the solar wind dynamic pressure was $P_{dyn} > 0.7$ nPa and group 2 contains the cases where the solar wind dynamic pressure was $P_{dyn} < 0.7$ nPa. 0.7 nPa corresponds to the typical slow solar wind of $v_{sw} = 400$ km/s

and $n_{sw} = 5$ cm^{-3} Table 1 lists the orbit number, the CENA sector number (sector 3 is the center sector), the lunar magnetic field strength measured at an altitude of 30 km by the Lunar Prospector magnetometer, the solar wind dynamic pressure, the solar wind magnetic field pressure, the observed shielding efficiency and the uncertainty of the shielding efficiency (as explained above) for the observations in group 1. We arranged the data in order of decreasing lunar magnetic field strength.

[13] Table 2 also lists the orbit number, the sector number, the lunar magnetic field strength at an altitude of 30 km, the solar wind dynamic pressure, the solar wind magnetic field pressure, the shielding efficiency and the uncertainty of the shielding efficiency, this time for the observations in group 2.

[14] Figure 4a presents a visualization of the data in Tables 1 and 2. The filled circles represent the shielding efficiency for group 1 and the empty circles represent the shielding efficiency for group 2. The error-bars show the uncertainty in the shielding efficiency. For a discussion of the accuracy of the magnetic field measurements we refer to *Richmond and Hood* [2008]. As one can see from the two tables and the corresponding plot, there does not seem to be an obvious correlation between the lunar magnetic field strength and the shielding efficiency. However, the shielding
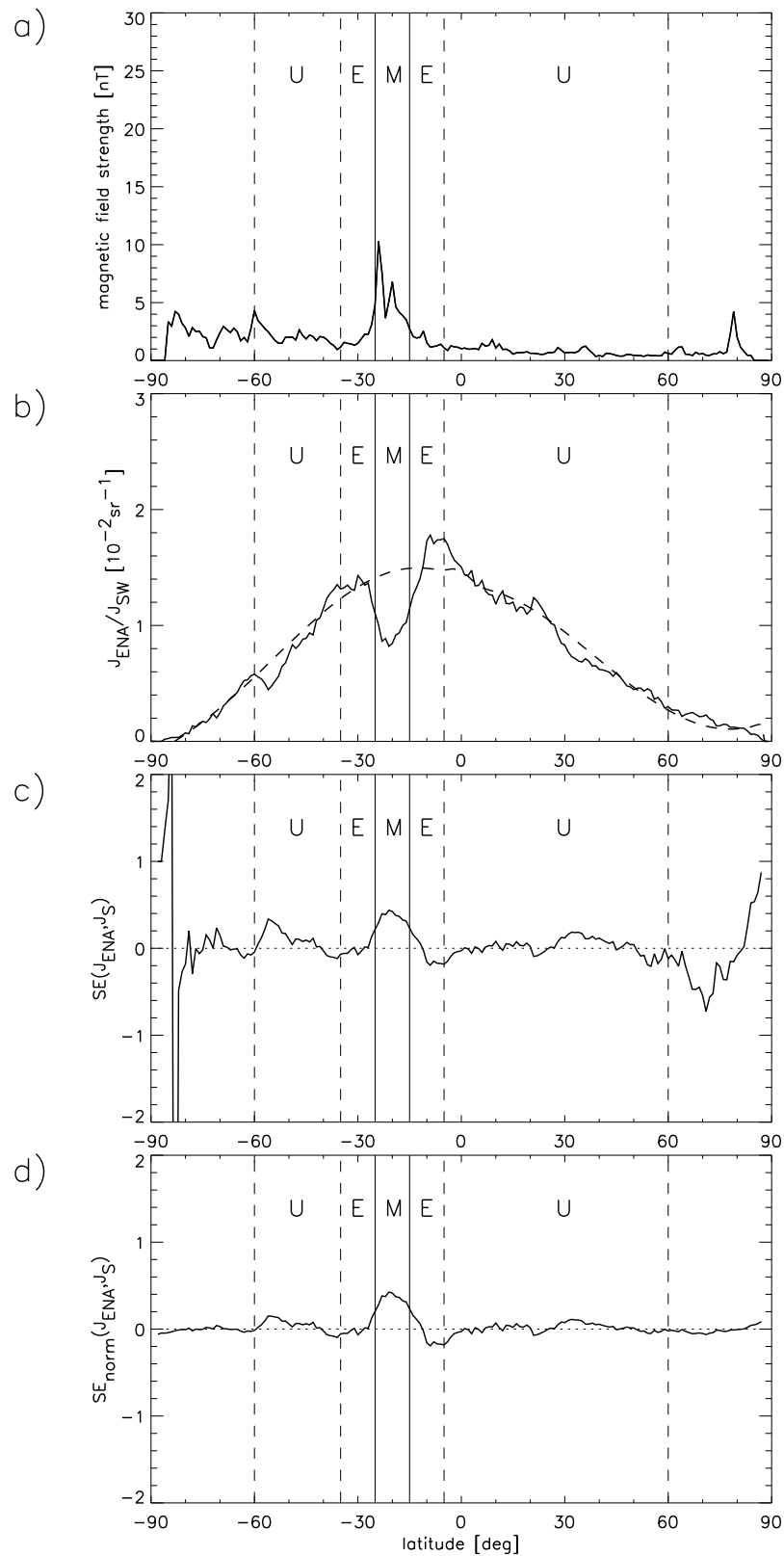
Figure 3. Computation of the shielding efficiency for orbit 2659 (17 June 2009 20:53:27–23:01:00) versus lunar latitude. (a) The lunar magnetic field as measured by the Lunar Prospector magnetometer at an altitude of 30 km. The labels 'U','M' and 'E' indicate the undisturbed, the minimagnetosphere, and the enhanced flux regions, respectively. (b) The normalized ENA flux (solid) and the corresponding amplitude fitted scattering function (dashed). (c) The shielding efficiency $SE(J_{ENA}, J_S)$ and (d) the normalized shielding efficiency $SE_{norm}(J_{ENA}, J_S)$.

Table 1. Shielding Efficiencies for All Observations of the Magnetic Anomaly Near the Gerasimovich Crater When the Solar Wind Dynamic Pressure Was Larger Than 0.7 nPa

Orbit	Sector	B_{30km} (nT)	P_{dyn} (nPa)	P_{mag} (nPa)	Shielding (%)	Uncertainty (%)
2021	2	17.50	1.928	0.016	30.89	11.13
2021	3	16.66	1.932	0.016	15.89	13.55
2018	1	14.64	1.181	0.010	18.20	15.64
2018	2	13.07	1.181	0.010	5.60	10.00
2021	4	13.07	1.958	0.016	32.95	9.85
2021	5	9.97	1.925	0.016	2.47	13.62
2021	1	8.81	1.925	0.016	46.91	13.45
2018	3	7.32	1.141	0.011	15.76	14.60
2018	4	6.37	1.206	0.010	2.12	6.33

efficiency appears to be anti-correlated with the solar wind dynamic pressure. As mentioned above, the further away the sectors are from the center sector, the larger the surface projected field-of-view. Because the magnetic anomaly structure on the surface is smaller than the surface projected fields-of-view of sectors 1 and 5, we decided to exclude these two sectors in a second attempt to organize the data. Figure 4b represents again the shielding efficiency and uncertainty for the two groups, but this time only for sectors 2–4. This plot shows that there does seem to be a correlation between the magnetic field strength of the anomaly and the shielding efficiency. To determine the degree of correlation we computed the Pearson correlation coefficient which is defined as the covariance of two variables (magnetic field strength and shielding efficiency, in our case) divided by the product of their standard deviations. The Pearson correlation coefficient ranges from -1 to 1. A value of 1 implies that the variables are positive correlated, 0 that they are uncorrelated,

and -1 implies that the variables are negative correlated. The Pearson coefficients for groups 1 and 2 are 0.77 and 0.56, respectively. We fitted the data of the Gerasimovich crater for the two groups with two straight lines, which are shown in Figure 4b and which have the following parametrization:

$$SE = -4.36 + 3.81 \cdot B_{moon}, \text{with R} = 0.79 \text{ for } P_{dyn} < 0.7 \text{ nPa},$$

$$SE = -9.27 + 2.09 \cdot B_{moon}, \text{with R} = 0.72 \text{ for } P_{dyn} > 0.7 \text{ nPa},$$

where R is the linear correlation coefficient and where P_{dyn} is the solar wind dynamic pressure.

[15] In addition to the correlation between the magnetic field strength and the shielding efficiency, at similar magnetic field strengths, group 1 shows clearly smaller shielding
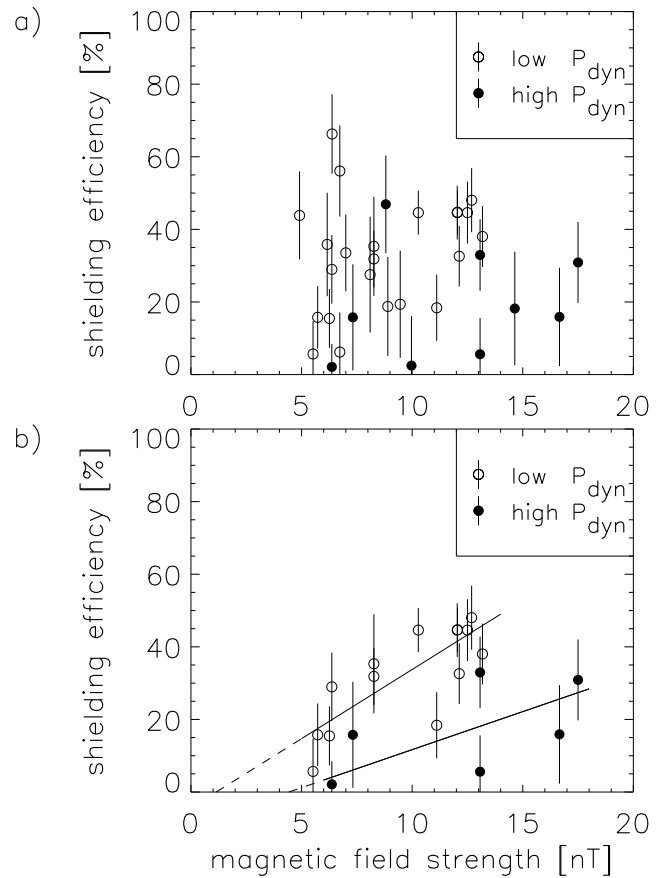
Table 2. Shielding Efficiencies for All Observations of the Magnetic Anomaly Near the Gerasimovich Crater When the Solar Wind Dynamic Pressure Was Less Than 0.7 nPa

Orbit	Sector	B_{30km} (nT)	P_{dyn} (nPa)	P_{mag} (nPa)	Shielding (%)	Uncertainty (%)
2659	3	13.18	0.608	0.006	38.03	8.38
2658	3	12.69	0.570	0.007	48.04	8.82
2657	2	12.50	0.479	0.007	44.61	8.52
2657	3	12.13	0.479	0.007	32.60	8.35
2658	2	12.05	0.575	0.007	44.71	6.11
2659	2	12.04	0.608	0.006	44.60	7.41
2964	4	11.11	0.659	0.002	18.40	9.10
2659	4	10.28	0.601	0.006	44.61	6.06
2964	5	9.46	0.656	0.002	19.38	14.77
2650	1	8.90	0.616	0.013	18.77	13.63
2658	4	8.27	0.570	0.007	31.86	7.82
2964	3	8.27	0.672	0.002	35.32	13.64
2648	1	8.10	0.533	0.011	27.53	15.94
2657	1	7.00	0.479	0.007	33.53	10.59
2961	5	6.73	0.589	0.004	6.21	10.92
2964	1	6.73	0.658	0.002	56.08	12.54
2658	1	6.38	0.574	0.007	66.27	10.96
2657	4	6.37	0.479	0.007	28.97	9.45
2961	4	6.26	0.595	0.004	15.46	8.10
2030	5	6.16	0.570	0.008	35.85	14.25
2964	2	5.73	0.688	0.002	15.77	8.60
2961	3	5.52	0.588	0.004	5.68	9.06
2659	1	4.91	0.602	0.006	43.83	12.12

Figure 4. Shielding efficiency versus magnetic field strength for the available Gerasimovich anomaly (location number 9) observations. Figure 4a shows the measurements of sectors 1–5 whereas Figure 4b only shows the measurements conducted by sectors 2–4. The empty circles present the data which was measured under low solar wind dynamic pressure conditions (< 0.7 nPa) and the filled circles present the data taken under high solar wind dynamic pressure conditions (> 0.7 nPa). The error-bars correspond to the variance of the normalized shielding efficiency $SE_{norm}(J_{ENA}, J_S)$ in the undisturbed region 'U'. The two straight lines in Figure 4b point out the correlation between the magnetic field strength and the shielding efficiency.

Table 3. Shielding Efficiencies for the Observations of the Remaining Locations (1, 2, 3, 5, 6, 7, 8, 10) for Sectors 2–4

Location	Orbit	Sector	B_{30km} (nT)	P_{dyn} (nPa)	P_{mag} (nPa)	Shielding (%)	Uncertainty (%)
1	1981	3	8.57	0.573	0.003	6.14	17.77
1	2930	3	5.47	0.393	0.002	40.36	15.37
1	2930	2	5.14	0.394	0.002	31.45	11.75
1	2930	4	4.29	0.363	0.002	34.29	14.53
2	1957	2	6.05	0.576	0.005	17.80	11.00
3	2601	2	5.20	0.499	0.001	1.39	12.70
3	2599	2	5.06	0.383	0.006	4.50	5.51
3	1957	2	5.01	0.685	0.005	25.55	11.00
5	1908	4	4.79	1.077	0.007	41.48	12.41
6	3026	3	10.34	0.734	0.015	57.65	6.78
6	3025	3	10.20	1.236	0.017	74.26	12.60
6	3022	2	9.62	0.778	0.005	49.41	5.73
6	3025	4	9.54	1.184	0.019	55.64	5.98
6	3026	2	9.08	0.805	0.016	54.87	7.77
6	3022	3	8.86	0.784	0.005	63.35	8.00
6	3022	4	8.53	0.779	0.005	48.09	5.73
6	3025	2	8.53	1.215	0.017	55.34	9.17
6	3026	4	7.75	0.785	0.016	34.44	7.20
6	2428	4	7.32	0.981	0.016	46.39	8.35
6	2428	3	6.14	0.996	0.016	27.38	6.95
7	3001	4	6.77	0.463	0.001	61.29	7.37
7	3000	4	6.59	0.437	0.001	55.62	9.15
7	3001	3	6.32	0.463	0.001	52.43	6.33
7	2997	3	6.09	0.377	0.001	54.07	8.12
7	3000	3	5.90	0.431	0.001	65.12	7.39
7	2997	4	5.88	0.373	0.001	56.70	7.31
7	3000	2	5.88	0.437	0.001	42.34	9.00
7	3001	2	5.72	0.464	0.001	50.42	6.04
7	2997	2	4.96	0.376	0.001	40.37	6.88
7	2992	4	4.33	0.322	0.002	13.47	5.17
8	2997	3	5.48	0.370	0.001	49.24	8.12
8	2997	2	5.23	0.369	0.001	21.85	6.88
8	2992	4	4.53	0.314	0.002	15.98	5.17
8	2997	4	4.20	0.370	0.001	17.82	7.31
8	2992	3	4.04	0.314	0.002	13.18	7.83
10	2946	2	4.80	0.604	0.002	54.84	35.15
10	2947	2	4.49	1.284	0.007	33.88	5.44
10	2946	3	4.43	0.594	0.002	64.70	32.09

Figure 5. Shielding efficiency versus magnetic field strength for all locations except the Gerasimovich anomaly (location number 9). The different symbols indicate to which location each measurement belongs. The location numbers correspond to the numbers presented in Figure 1. No data point is available for location number 4. For locations 6, 7, and 8 we fitted a straight line which highlights the correlation between the magnetic field strength and the shielding efficiency.

[17] There is a clear correlation between the surface magnetic field strength and the shielding efficiency observable for locations 6 (Imbrium basin antipode), 7 (Serenitatis basin antipode) and 8 (northeast of Serenitatis basin

Table 4. Shielding Efficiencies for the Observations of the Remaining Locations (1, 2, 3, 5, 6, 7, 8, 10) for Sectors 1 and 5

Location	Orbit	Sector	B_{30km} (nT)	P_{dyn} (nPa)	P_{mag} (nPa)	Shielding (%)	Uncertainty (%)
2	2599	1	5.43	0.389	0.006	13.22	16.73
2	2598	1	5.25	0.475	0.002	13.42	18.40
2	2608	5	5.11	0.620	0.003	15.38	13.86
2	2601	1	4.87	0.520	0.001	25.80	20.79
4	1910	5	7.07	1.119	0.008	14.33	12.80
4	1908	5	5.92	1.118	0.007	26.13	19.23
5	1909	5	6.18	1.055	0.006	42.10	25.72
5	1908	5	5.91	1.081	0.007	39.61	19.23
5	1910	5	4.86	1.017	0.008	42.08	12.80
6	3022	1	8.40	0.775	0.005	69.86	14.37
6	3025	1	7.84	1.229	0.017	58.54	14.95
6	3022	5	7.54	0.780	0.005	52.23	7.91
6	3026	5	7.32	0.738	0.015	52.26	10.16
6	3026	1	7.08	0.820	0.016	52.64	10.53
6	3025	5	6.83	1.169	0.019	65.29	15.34
6	2428	5	6.45	0.999	0.016	49.74	8.88
7	3001	5	5.33	0.464	0.001	59.88	11.12
7	3000	5	5.31	0.427	0.001	50.88	11.71
7	3001	1	5.15	0.465	0.001	48.01	14.72
7	2997	5	5.08	0.373	0.001	46.60	9.70
7	3000	1	5.08	0.430	0.001	36.16	16.48
7	2997	1	4.79	0.377	0.001	49.66	14.46
7	2992	5	4.09	0.322	0.002	22.53	7.04
8	2045	1	4.77	0.571	0.013	18.74	20.21
10	2946	1	4.13	0.600	0.002	58.09	36.16
10	2947	1	4.13	1.292	0.008	42.94	10.48

efficiencies than group 2, which indicates that the solar wind dynamic pressure also influences the shielding efficiency.

[16] Based on these findings, we chose to only consider the ENA signals measured by sectors 2–4 in the analysis of the other magnetic anomalies. Also, we only present the data where a magnetic anomaly signature is visible in the ENA signal. Due to this constraint, we unfortunately do not have any valid observations for location number 4 (Airy crater). Out of a total of 85 observations, 64 showed a magnetic anomaly signature. 38 of these observations were conducted by sectors 2–4. Table 3 presents the orbit number, the sector number, the lunar magnetic field strength at an altitude of 30 km, the solar wind dynamic pressure, the solar wind magnetic field pressure, the shielding efficiency and the uncertainty of the shielding efficiency for these 38 observations. We present the shielding efficiency and the uncertainty thereof (as error-bars) as a function of magnetic field strength in Figure 5. The different symbols indicate to which surface location a certain measurement belongs. For reason of completeness, even though we do not use these data in our analysis, we present in Table 4 the observations conducted by sectors 1 and 5 of all locations except the Gerasimovich anomaly.
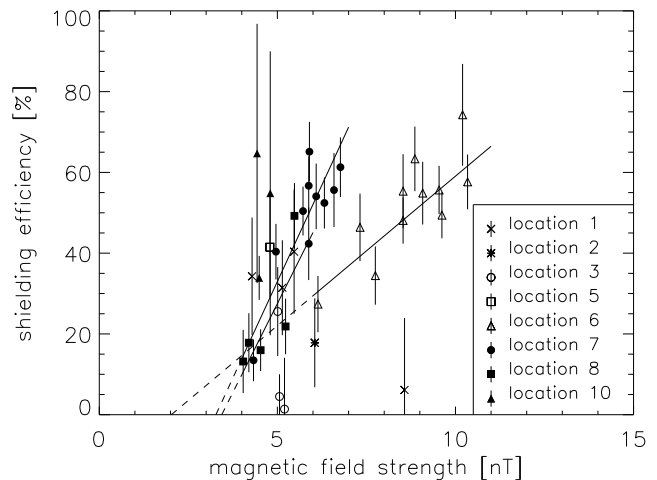
antipode). The values of the Pearson correlation coefficient for these three locations are 0.82, 0.84 and 0.81, respectively. Again, we fitted the data of the three locations with straight lines which are shown in Figure 5 and which have the following parametrization:

$$SE = -14.97 + 7.40 \cdot B_{\text{moon}}, \text{with R} = 0.82 \text{ for location } 6,$$

$$SE = -62.61 + 19.12 \cdot B_{\text{moon}}, \text{with R} = 0.90 \text{ for location } 7,$$

$$SE = -60.57 + 17.61 \cdot B_{\text{moon}}, \text{with R} = 0.78 \text{ for location } 8.$$

[18] Unfortunately, there are not enough data points for locations number 2 (Reiner Gamma) and 5 (crater Stöfler) to make a statement concerning the relationship between the magnetic field strength and the shielding efficiency. For locations 1 (crater Hartwig), 3 (Rima Sirsalis), and 10 (Mendel-Rydberg basin) there is no correlation visible between the magnetic field strength and the shielding efficiency. As it turned out most observations of the remaining anomalies were conducted under similar solar wind conditions. We therefore were not able to split the observations of the individual anomalies up into two groups as we did in the Gerasimovich case. In any event, since the structures of the different magnetic anomalies show plenty of small-scale magnetic field structure, these results would be much more difficult to interpret than the results obtained in the Gerasimovich case. We therefore cannot make any conclusions on the influence of the solar wind dynamic pressure on the shielding efficiency based on these observations.

5. Discussion and Conclusion

[19] When interpreting our results, one has to keep in mind, that the data analysis was done fully automatic. The magnetic anomaly signature, which corresponds to a reduction in the measured ENA flux, can be due to either magnetic surface shielding or to different backscattering efficiencies corresponding to different surface structures and mineralogical compositions. The effects of these two causes overlap and we can therefore not determine which cause is responsible for an observed ENA flux reduction. We therefore chose to only analyze measurements where the location of the observed reduction in ENA flux exactly corresponds to a location where the Lunar Prospector magnetometer measured a drastic increase in magnetic field strength. Nevertheless, it is possible that we mistook a coincidental depression in the signal above an anomaly as a shielding signature. However, given the large number of positive detections of ENA suppression at magnetic anomalies and the observed correlations with the solar wind dynamic pressure (see Figure 4b) and the lunar surface magnetic field (see Figure 5), we are convinced that in most cases we have a true identification.

[20] CENA conducted 121 observations of 10 different magnetic anomalies on the lunar surface. One of the locations (number 4) had to be excluded, because it was only observed by the outermost sectors, for which the footprint on the lunar surface is too large to be useful for further analysis. For 4 out of the remaining 9 locations, a clear correlation between the local lunar magnetic field strength and the reduction in the reflected ENA flux was observed.

For two locations (numbers 2 and 5) we had only one valid data point remaining and could therefore not analyze if a correlation exists. The remaining 3 locations did not exhibit a correlation between the local lunar magnetic field strength and the reduction in the reflected ENA flux. For the simplest lunar magnetic structure, i.e., the magnetic anomaly near the Gerasimovich crater, for which we also have by far the largest number of observations, an anti-correlation between the solar wind dynamic pressure and the reduction in reflected ENA flux was also observable.

[21] Three out of the four locations, which showed a correlation between the local magnetic field strength and the reduction in reflected ENA flux, are very large in size compared to the other locations where we did not detect such a correlation. The gyroradius of a typical solar wind proton (E_{sw} = 1 keV, v_{sw} = 439 km/s) in a lunar magnetic field of 30 nT, which is the highest value measured by the Lunar Prospector magnetometer at an altitude of 30 km, is 152 km. This corresponds to a surface extension of 5° in lunar coordinates. Of course, at the surface, the maximal magnetic field strength will be higher than at an altitude of 30 km, and the actual surface gyroradius will therefore be smaller. As one can see from Figure 1, the size of the high magnetic field region at the Gerasimovich crater (location number 9) is therefore equal to at least 2–3 gyroradii. The anomaly near the South Pole - Aitken basin (location number 6) and the anomaly near the Serenitatis antipode (location number 7) have dimensions of at least 6 and 2.5 gyroradii, respectively, but have magnetic field structures of smaller scale. The anomaly slightly north-east of the Serenitatis antipode (location number 8) only has a diameter of at least 1 gyroradius. When the magnetic anomalies are larger than the local gyroradii, the deflection of the solar wind by the magnetic field can be understood in a similar way as for the larger magnetospheres, e.g. Earth's magnetosphere. However, when the anomalies are of comparable size as the gyroradius the classical interaction between solar wind plasma and the magnetic field obstacle does not apply anymore. From our observations, we have learned that magnetic anomalies, which are at an altitude of 30 km of comparable size as the gyroradius, are presenting an obstacle to the solar wind plasma. To understand the actual plasma physics detailed modeling will have to be developed that reproduces the range of observation, i.e., either a correlation with the surface magnetic field (e.g. location number 8) or no correlation (e.g. locations number 3 and 10).

[22] Gerasimovich was the only location for which we had a sufficient number of measurements conducted under low and under high solar wind dynamic pressure conditions to analyze the influence on the dynamic pressure on the shielding efficiency. The shielding efficiency is found to be higher when the solar wind dynamic pressure is lower. This agrees with the theory that the minimagnetosphere is established, to a first order, by the pressure balance between the solar wind dynamic pressure and the crustal magnetic field pressure. When the solar wind pressure increases the minimagnetosphere becomes smaller and more ions are able to penetrate the minimagnetosphere.

[23] We also looked at the angle between the interplanetary magnetic field and the local magnetic field to see if the shielding efficiency increases for favorable conditions. Whereas the total lunar magnetic field already shows

significant spatial variation, the three components (radial, north, east) show even more spatial variation. We find that the angle between the solar wind magnetic field and the lunar magnetic field at the point of observation changes too frequently that a useful mean value can be given for the observation of one orbit's region 'M'. Because of the high fluctuation in the angle between the magnetic fields it is impossible to search for a correlation between the interplanetary magnetic field - local magnetic field angle and the shielding efficiency.

[24] Our analysis of the available magnetic anomaly observations by CENA shows that several magnetic anomalies on the lunar surface are able to produce minimagnetospheres, which can to a certain degree deflect the impinging solar wind. The degree to which a minimagnetosphere is able to deflect the solar wind depends on the surface magnetic field strength and the solar wind dynamic pressure. These results should be helpful in identifying which magnetic anomalies are worth studying under what conditions to gain further insight into the plasma physics behind minimagnetosphere. Candidates of interest are for example the other magnetic anomalies on the Moon that have not been analyzed in this paper, the magnetic anomalies on Mars and the magnetic field of Ganymede, a mission to which is already being planed.

[25] To investigate the shielding of minimagnetospheres, as they exist on the Moon, one has to take not only the local magnetic field strength and solar wind dynamic pressure into account, but also other influences such as the geometric extend of the magnetic field, the magnetic field structure, the solar wind incidence angle, the angle between the interplanetary magnetic field and the local magnetic surface field, the direction of the surface magnetic field and surface structural and/or mineralogical inhomogeneities. In the case of the Moon, one problem that arises is that the magnetic anomalies are highly structured on a very small spatial scale. The Gerasimovich anomaly showed to be a simple, large scale structure, which was observed under favorable conditions. Usually, the interaction process seems to be more complex, though. To investigate the interaction between the solar wind plasma and the minimagnetospheres more thoroughly, an instrument with even higher spatial and temporal resolution is required and locally detailed 3D kinetic models of the plasma physical processes are needed for interpretation.

References

Barabash, S., et al. (2009), Investigation of the solar wind-moon interaction onboard Chandrayaan-1 mission with the SARA experiment, *Curr. Sci.*, *96*(4), 526–532.

Bhardwaj, A., S. Barabash, Y. Futaana, Y. Kazama, K. Asamura, R. Sridharan, M. Holmström, P. Wurz, and R. Lundin (2005), Low energy neutral atom imaging on the moon with the sara instrument aboard Chandrayaan-1 mission, *J. Earth Syst. Sci.*, *114*(6), 749–760, doi:10.1007/BF02715960.

Dyal, P., C. Parkin, and C. Sonett (1970), Apollo 12 magnetometer: Measurement of a steady magnetic field on the surface of the Moon, *Science*, *21*, 762–764, doi:10.1126/science.169.3947.762.

Dyal, P., C. Parkin, C. Snyder, and D. Clay (1972), Measurements of lunar magnetic field interaction with the solar wind, *Nature*, *236*, 381–385, doi:10.1038/236381a0.

Futaana, Y., S. Barabash, M. Holmström, and A. Bhardwaj (2006), Low energy neutral atoms imaging of the Moon, *Planet. Space Sci.*, *54*, 132–143, doi:10.1016/j.pss.2005.10.010.

Futaana, Y., S. Barabash, M. Wieser, M. Holmstrm, C. Lue, P. Wurz, A. Schaufelberger, A. Bhardwaj, M. Dhanya, and K. Asamura (2012), Empirical energy spectra of neutralized solar wind proton from the lunar regolith, *J. Geophys. Res.*, *117*, E05005, doi:10.1029/2011JE004019.

Goswami, J., and M. Annadurai (2009), Chandrayaan-1: India's first planetary science mission to the Moon, *Curr. Sci.*, *96*(4), 486–491.

Harnett, E. M., and R. M. Winglee (2002), 2.5D particle and MHD simulations of mini-magnetospheres at the Moon, *J. Geophys. Res.*, *107*(A12), 1421, doi:10.1029/2002JA009241.

Kurata, M., H. Tsunakawa, Y. Saito, H. Shibuya, M. Matsushima, and H. Shimizu (2005), Mini-magnetosphere over the reiner gamma magnetic anomaly region on the Moon, *Geophys. Res. Lett.*, *32*, L24205, doi:10.1029/2005GL024097.

Lin, R., D. Mitchell, D. Curtis, K. Anderson, C. Carlson, J. McFadden, M. Acuña, L. Hood, and A. Binder (1998), Lunar surface magnetic fields and their interaction with the solar wind: Results from lunar prospector, *Science*, *281*, 1480–1484, doi:10.1126/science.281.5382.1480.

Mitchell, D., J. Halekas, R. Lina, S. Freya, L. Hood, M. Acuña, and A. Binder (2008), Global mapping of lunar crustal magnetic fields by lunar prospector, *Icarus*, *194*, 401–409, doi:10.1016/j.icarus.2007.10.027.

Richmond, N., and L. Hood (2008), A preliminary global map of the vector lunar crustal magnetic field based on lunar prospector magnetometer data, *J. Geophys. Res.*, *113*, E02010, doi:10.1029/2007JE002933.

Runcorn, S., D. Collinson, W. O'Reilly, A. Stephenson, N. Greenwood, and M. Battey (1970), Magnetic properties of lunar samples, *Science*, *30*, 697–699, doi:10.1126/science.167.3918.697.

Russell, C., and B. Lichtenstein (1975), On the source of lunar limb compressions, *J. Geophys. Res.*, *80*(34), 4700–4711, doi:10.1029/JA080i034p04700.

Schaufelberger, A., P. Wurz, S. Barabash, M. Wieser, Y. Futaana, M. Holmström, A. Bhardwaj, M. Dhanya, R. Sridharan, and K. Asamura (2011), Scattering function for energetic neutral hydrogen atoms off the lunar surface, *Geophys. Res. Lett.*, *38*, L22202, doi:10.1029/2011GL049362.

Wieser, M., S. Barabash, Y. Futaana, M. Holmström, A. Bhardwaj, R. Sridharan, M. Dhanya, A. Schaufelberger, P. Wurz, and K. Asamura (2010), First observation of a mini-magnetosphere above a lunar magnetic anomaly using energetic neutral atoms, *Geophys. Res. Lett.*, *37*, L05103, doi:10.1029/2009GL041721.